Available online at www.sciencedirect.com

SciVerse ScienceDirect

Acta Materialia 60 (2012) 1193–1200

Acta MATERIALIA

www.elsevier.com/locate/actamat

In situ micro-cantilever tests to study fracture properties of NiAl single crystals

F. Iqbal, J. Ast, M. Göken, K. Durst *

Department of Materials Science and Engineering, Institute I: General Materials Properties, Friedrich-Alexander-University of Erlangen-Nuremberg, Germany

Received 20 July 2011; accepted 31 October 2011
Available online 15 December 2011

Abstract

In situ micro-cantilever tests were carried out to determine the anisotropic fracture toughness of NiAl single crystals. Notched micro-cantilever beams with a beam length of 8 μm, 1.5 μm thickness and 1.8 μm width were milled in so-called "hard" and "soft" orientations of NiAl using a focused ion beam. These cantilevers were loaded in situ with the help of a cantilever-based nanoindenter mounted inside a scanning electron microscope. A fracture toughness of 3.52 ± 0.29 MPa $m^{1/2}$ was obtained for the "soft" orientation and 5.12 ± 0.50 MPa $m^{1/2}$ for the "hard" orientation, which is in good agreement with literature values on the fracture toughness of macroscopic NiAl specimens. Furthermore, nanoindentations were performed for studying the size effects occurring at small length scales for both orientations. The applicability of the small sample geometries for testing the fracture toughness is finally discussed in terms of size effects in the flow stress of the material due to dislocation nucleation and strain gradients at the crack tip.

Keywords: Fracture toughness; In situ micro-cantilever testing; NiAl; Strain gradients

1. Introduction

Nanomechanical testing is nowadays important for studying the material properties at the micron or even sub-micron scale. Different methods like nanoindentation [1–3], micro-tensile [4–6], bulge [7,8], micro-compression [9,10] and notched micro-cantilever fracture tests [11,12] are used on various material systems. Nanoindentation has already proved to be a very versatile method to determine the local hardness and the reduced modulus on the sub-micron scale. Pre-notched micro-cantilever samples were investigated for some materials like SiO_2/metal interfaces [13], nitride and oxynitride coatings [12], and TiAl alloys [6,14]. Metallic materials like TiAl alloys are quite complex as they have a multiphase microstructure and exhibit anisotropic elastic–plastic deformation behavior. Therefore a thorough investigation of different metallic materials is necessary to understand the microscopic fracture toughness mechanisms and their relation to macroscopic tests. Halford et al. [11] carried out ex situ micro-cantilever tests on lamellar TiAl alloys to measure the fracture toughness. They found that the fracture toughness at the micron scale is lower although the data scatter is relatively large. The decisive toughness reduction was explained by a reduction in shear ligament bridging, which causes extrinsic toughening in TiAl alloys.

In order to investigate and to understand the relation between micron scale fracture toughness and that of bulk materials, we carried out in situ micro-cantilever tests on notched NiAl single crystals. NiAl is brittle at ambient temperature and the macroscopic fracture toughness K_{IC} has been already investigated intensively and reported in the literature [15–17]. The fracture toughness K_{IC} of NiAl is anisotropic, and "hard" and "soft" orientations are discussed separately. The macroscopic fracture toughness K_{IC} measured using ASTM 399 standard ranges from 3 to 4 MPa $m^{1/2}$ for specimens which were loaded along the

* Corresponding author.
E-mail address: karsten.durst@ww.uni-erlangen.de (K. Durst).

1359-6454/$36.00 © 2011 Acta Materialia Inc. Published by Elsevier Ltd. All rights reserved.
doi:10.1016/j.actamat.2011.10.060

⟨1 1 0⟩ direction, i.e. in the "soft" orientation of NiAl [16]. A K_{IC} value of 5–7 MPa $m^{1/2}$ is reported when the crystal is loaded along the ⟨1 0 0⟩ orientation, which is the "hard" orientation of NiAl [15]. The cleavage fracture occurs at the (1 1 0) planes, unlike other body centered materials like α-Fe, W, Cr, etc. [16,17]. In this work the micro-cantilever method as introduced by Maio et al. [14] and Halford et al. [11] was used to investigate the orientation-dependent fracture toughness of NiAl at the micron scale. Its relation to the macroscopic fracture toughness is also discussed. The versatility of the micro-cantilever deflection technique is shown and the results are discussed in light of the linear-elastic fracture mechanics and the dislocation nucleation and mobility in NiAl, together with strain gradient plasticity effects at the crack tip.

2. Experimental details

2.1. Material and specimen preparation

A focused ion beam (FIB) (Crossbeam Gemini 1540, Carl Zeiss, Germany) was used to mill NiAl micro-cantilever beams in both "soft" and "hard" orientations. The orientations of the samples were confirmed to deviate less than 5° from the "soft" and "hard" orientations using electron back-scattered diffraction (EBSD) in the FIB. The cantilever beams with a nominal beam length of 8 μm, a width of 1.8 μm and a thickness of 1.5 μm were coarsely milled with a high current Ga^+-ion beam (30 keV, 10 nA, 2 nA and 500 pA), followed by fine milling at low currents (30 keV, 20–200 pA). The cantilevers were notched using an even finer milling current (30 keV, 5 pA), at a distance of 2 μm away from the cantilever beam support. The depths of the pre-notches were measured prior to fracture from the side view; in some cases notches were measured after fracture as well when the cantilever was completely fractured apart. As a consequence of the FIB-milling from the side, the crack tip is slightly rounded and not atomistically sharp. This might possibly lead to an overestimation of the fracture toughness. In total 11 cantilevers, six on the "soft" and five on the "hard" orientations, were tested in the in situ beam bending experiments. The notch tip radius a_{ct} is in the range of 70–120 nm (Fig. 1).

The loading of the cantilever beams is carried out using a force measurement system (FMS), from Kleindiek Nanotechnik, Germany. The FMS is fitted to a micromanipulator, which provides three-dimensional flexibility to position the cantilever-based indenter. The FMS is equipped with a 120 μm long cantilever that is coated with a piezo-resistive coating which generates a voltage signal upon bending. This voltage signal was calibrated by bending a compliant copper needle with a stiffness of 9.36 μN $μm^{-1}$, which allows converting the voltage signal into a force signal.

The force resolution of the FMS system is ~1 μN. Loading of the micro-cantilever beams was carried out manually as the FMS system does not offer a software control for predefining the loading rates. Experiments with a controlled strain rate are thus not possible. Nevertheless the obtained K_{IC} values show relatively low scatter, as shown in Fig. 6. Hence the manual loading should have no remarkable effect on the measured values of fracture toughness.

Nanoindentations were performed using a Berkovich tip on a Nanoindenter XP (Agilent Technologies, USA). Tip shape calibration and machine stiffness were taken into account. The samples were ground using 2400 grit SiC paper followed by a chemical–mechanical polish with a mixture of 90 parts of colloidal silica (Struers OP-S) and 10 parts of hydrogen peroxide (30 vol.%). Finally the specimens were electrolytically polished to remove the residual deformation layers until subsequent polishing leads to the same nanoindentation response in terms of hardness and pop-ins.

2.2. Evaluation of fracture properties

The fracture toughness K_{IC} was calculated using the following equation:

$$K_{IC} = \frac{F_{\max} L}{B W^{3/2}} f(a/W) \tag{1a}$$

where $F_{\max}$ is the fracture force and $f(a/W)$ is a dimensionless geometry factor of the tested specimens [18]. The loading span L is the distance between the notch and the loading point, a is the crack length, W is the cantilever width and B is the thickness as shown in Figs. 1 and 2.

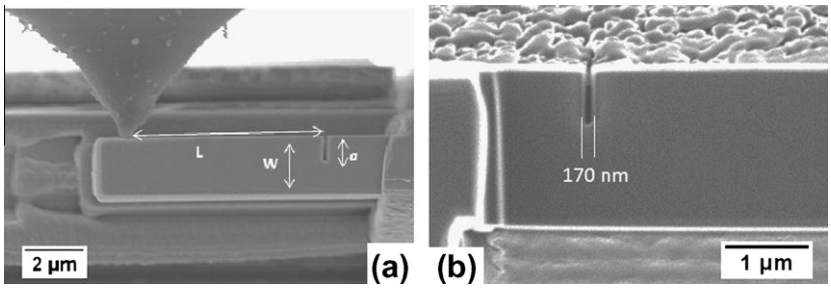

Fig. 1. (a) Notched micro-cantilever in contact with nanoindenter. L: bending span; W: thickness. (b) Magnification of FIB-made notch with a diameter of 170 nm.

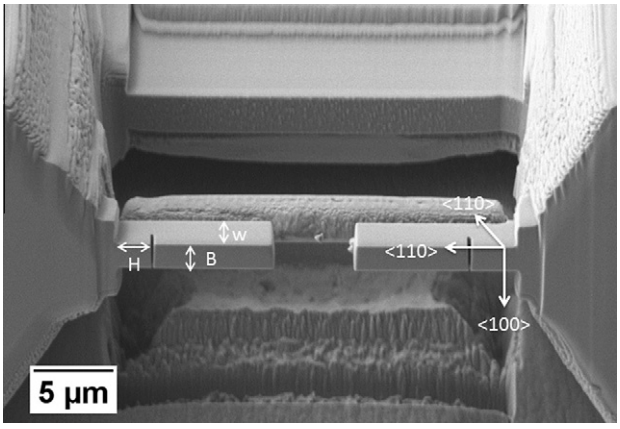

Fig. 2. FIB-prepared notched cantilevers of NiAl in "soft" ⟨110⟩ orientation.

The dimensionless geometry factors $f(a/W)$ for the different beam aspect ratios are determined by finite element modeling (FEM) using the commercial FE-solver ABAQUS. Two-dimensional (2-D) isotropic elastic material models with biquadratic plane strain elements (CPE8R) were used. Loading was applied by a concentrated point load at a distance of L from the crack (see Fig. 3a). First the model was optimized for getting mesh-independent results. A total of 15 contours were made around the crack tip and for each incremental loading step the values of stress intensity factor K_I from all 15 contours were extracted and averaged. Similarly for each increment the stiffness response of the cantilever was also recorded. Finally the K_I vs. force data were used to calculate the geometric factors $f(a/W)$:

$$f(a/W) = \frac{K_{IC} B W^{3/2}}{F_{\max} L} \tag{1b}$$

The simulations were performed for two different cantilever aspect ratios, ($H{:}L{:}W{:}B = 2{:}5{:}2.1{:}1.7$ [12] and $H{:}L{:}W{:}B = 2{:}5{:}2.1{:}1.3$) in order to determine the dimensional effects on the geometry factor f(a/w). Matoy et al. [12] suggested to use the calculated shape factors for specific aspect ratios ($H{:}L{:}W{:}B = 2{:}5{:}2.1{:}1.7$) of cantilever beams. However, during FIB preparation it is almost impossible to exactly control the beam dimensions. Therefore we chose different aspect ratios as well as different loading spans to see if these could affect the resultant geometry factor values. The calculated geometry factors $f(a/W)$ with their derived cubic polynomial fitting equations are shown in Fig. 3b. The measured geometry factors show very good agreement with literature values given in Ref. [12].

2.3. Specimen size effects on stress state in cantilever

For reliable fracture toughness tests the ratio of specimen thickness to the size of the plastic zone has to be considered. According to the ASTM standard the experimental model of Anderson [19] explains a possible variation of the measured fracture toughness according to the stress state in the cantilever. For specimens thinner than a critical thickness t_1, the plane-stress value $K_{IC}^{plane-stress}$ is measured, while the plane-strain value of K_{IC} requires a specimen size above a critical thickness t_2.

The size of the plastic zone t_1 is estimated according to the Irwin approximation [20] and is determined for both "hard" and "soft" orientations of NiAl using:

$$t_1 = \frac{K_{IC}^2}{3\pi\sigma_Y^2} \tag{2}$$

The yield stress σ_Y is taken from the literature [21,22] and has also been calculated from nanoindentation experiments.

The critical specimen thickness limit t_2, for plane-strain fracture toughness, has been experimentally elucidated in Ref. [18] and is given in:

$$t_2 = 2.5\frac{K_{IC}^2}{\sigma_Y^2} \tag{3}$$

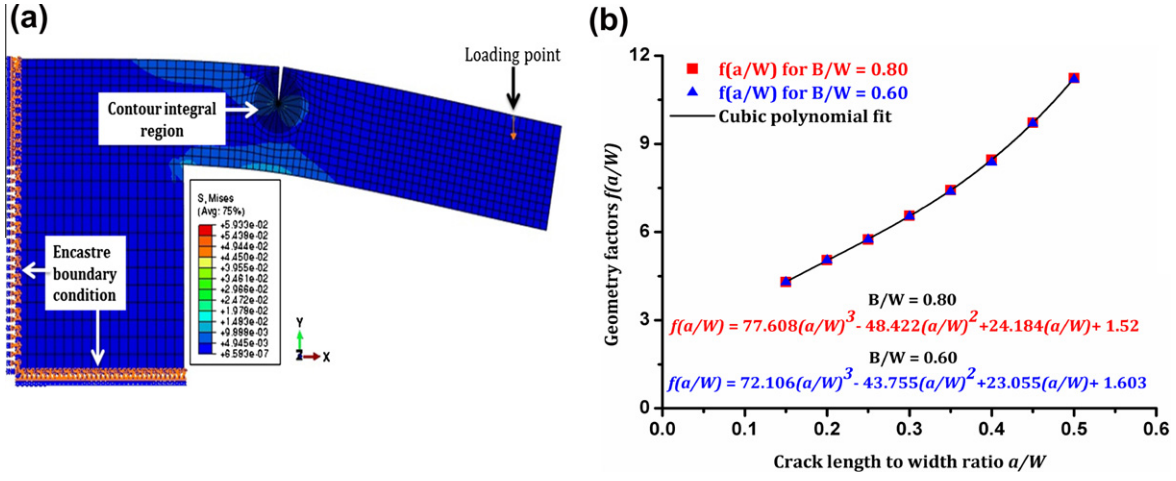

Fig. 3. 2-D finite element modeling for determination of geometry factor using J-integral method. (a) Model geometry with boundary conditions. (b) Geometry factors for cantilever beams with different B/W ratios plotted as a function of a/W (blue: $H{:}L{:}W{:}B = 2{:}5{:}2.1{:}1.3$, red: $H{:}L{:}W{:}B = 2{:}5{:}2.1{:}1.7$ [13].) (For interpretation of the references to colour in this figure legend, the reader is referred to the web version of this article.)

There is no accurate model which can either predict the ratio of $K_{IC}^{plane-stress}$ to K_{IC} or the slope of this transition. The approximation provided by Broek and Vlieger [23] can be used to assess the order of magnitude of this transition region with the help of

$$\frac{K_{IC}^{plane-stress}}{K_{IC}} = \sqrt{1 + \frac{\varepsilon_f E}{12\sigma_Y}} \quad (4)$$

where ε_f is the fracture strain of the material, E is the Young's modulus and σ_Y is the yield stress of the material. This model assumes a negligible transition for an ideal brittle material.

It is important to note that due to local strain gradients at the crack tip the local flow stress is not equivalent to the macroscopical material properties [24]. Size effects can lead to a significant increase in the flow stress of the material. For assessing the local flow stress of the material, nanoindentations were performed using a loading and unloading scheme, as described in Ref. [25]. It is assumed that similar size effects due to strain gradients are found at the crack tip as during the indentation of the material. Therefore the local yield stress of the material, acting at the crack tip, is estimated according to Tabor's approximation (Eq. (5)) [26]:

$$\frac{H}{\sigma_Y} \approx 3, \quad \text{here } C = 3 \quad (5)$$

where H is the hardness of the material and C is the constraint factor.

3. Results

3.1. Fracture toughness of "hard" and "soft" orientations

The FMS system is unable to record the relative displacement between the tip and the NiAl beam. Therefore in situ movies of all the tests were recorded in order to evaluate the force–displacement trend through image correlation software (VEDDAC 5.0, Chemnitzer Werkstoffmechanik, Germany). The force–displacement curves for tests on the "soft" and "hard" orientation are illustrated in Fig. 4. The corresponding in situ scanning electron microscopy (SEM) images of the loaded cantilever in the "soft" orientation are shown in Fig. 5. The force–displacement curve for the "soft" orientation shows initially a linear behavior, until a deviation occurs at a load of ~220 μN followed by a load drop at a force ~300 μN. The deviation from the linear regime is due to opening of the crack tip (see Fig. 5b). A similar crack tip opening was observed for loading–unloading tests on notched cantilevers. There the plastic deformation at the crack tip causes a permanent cantilever deformation after unloading. It should be noted that due to the limited amount of crack tip plasticity, linear elastic fracture mechanics is still applicable. After fracture, the crack runs straight through the material, with a small, still-intact ligament in the compression region of the beam. It should be noted that after cracking and unloading of the beam, the beam support remains undeformed. The force–displacement behavior for the "hard" orientation is slightly different. Crack initiation requires larger loads and the force–displacement data show a stiffer response. Moreover, the load–displacement data do not deviate from a straight line (or do so to a much smaller extent).

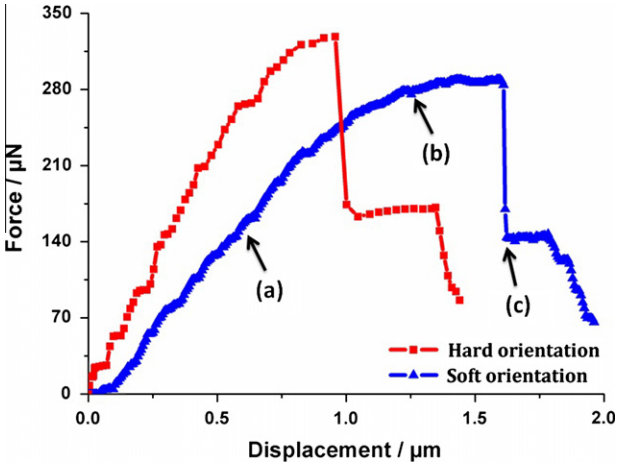

Fig. 4. Force–displacement curves for cantilever beams loaded in "soft" and "hard" orientation. Three regions are marked for the "soft" orientation with a (linear), b (non-linear) and c (force drop due to fracture). The corresponding in situ SEM images for the "soft" orientation are shown in Fig. 5.

The fracture toughness is evaluated using Eq. (1), where the maximum load F_{max} is taken from force–displacement data as shown in Fig. 5. The fracture toughness as measured with micro-cantilever tests and their comparison to literature values are presented in Fig. 6. The value of the fracture toughness is found to be 3.52 ± 0.29 MPa $m^{1/2}$ for the "soft" and 5.12 ± 0.50 MPa $m^{1/2}$ for the "hard" orientation. The measurements show a low scattering even though the FIB fabrication does not allow a constant beam geometry and notch radius.

Literature data for the fracture toughness of large samples, tested according to ASTM 399 standard are ~3–4 MPa $m^{1/2}$ [15–17,27] and 5–7 MPa $m^{1/2}$ [15–17] for "soft" and "hard" orientation, respectively. The micro-cantilever tests clearly show the orientation dependency of the fracture toughness and are moreover in good agreement with the macroscopic literature values. Theoretical values for the fracture toughness at 0 K are much smaller, compared to the experimental data, indicating that at room temperature, dislocation activity is contributing to the fracture toughness [28].

3.2. Indentation hardness and pop-in behavior

To estimate the local flow stress due to strain gradients, nanoindentations have been performed on both orientations. For the "hard" and "soft" orientation, indentations were performed along the ⟨100⟩ and ⟨110⟩ directions, respectively. The "hard" orientation shows elastic Hertzian behavior up to a load of ~800 μN, followed by a large pop-in in the load–displacement data (Fig. 7a). A pop-in

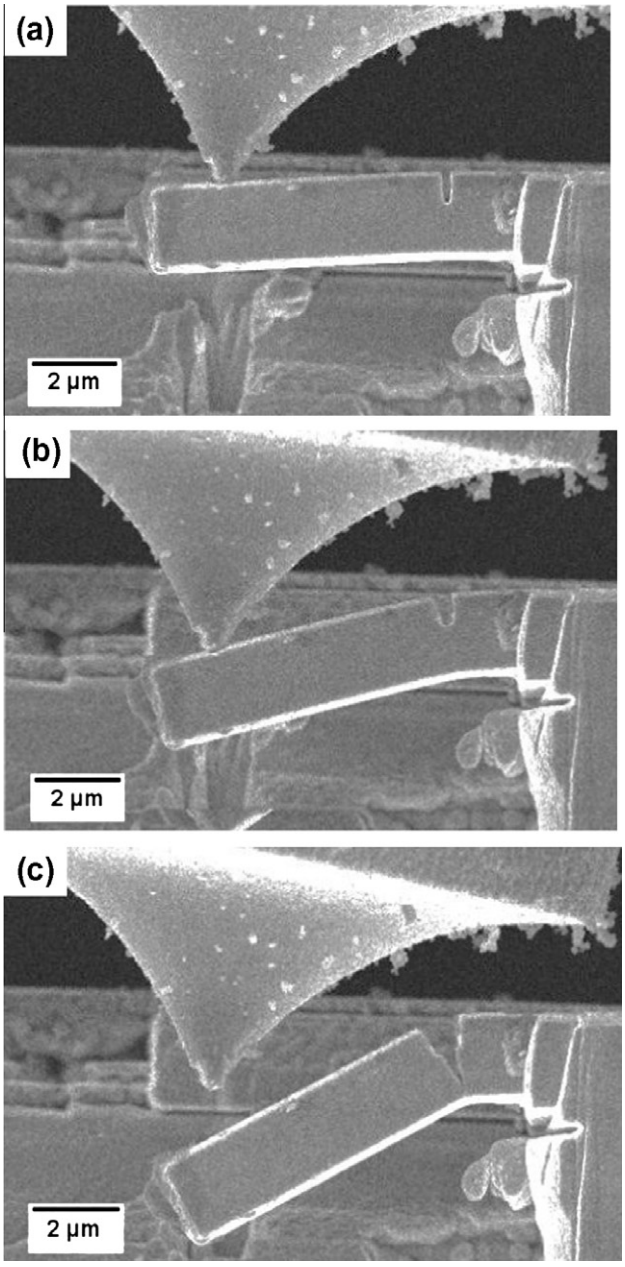

Fig. 5. In situ SEM images of a deflected "soft" oriented cantilever for the corresponding points in the force–displacement curve in Fig. 4: (a) linear elastic region, (b) crack tip opening, and (c) fracture.

is also observed for the "soft" orientation, but at a much smaller pop-in load of ~200 μN. The pop-in is a good indicator for dislocation nucleation, which requires a much larger stress for the "hard" orientation. In Fig. 7b the hardness as a function of indentation depth shows an indentation size effect, where the hardness declines with increasing indentation depth. Before pop-in, an elastic contact pressure of ~23 GPa is found for the hard orientation. The hardness values for both orientations are clearly depth-dependent, where a larger hardness is found at smaller depths. There the hardness nearly doubles compared to the plateau hardness value of ~2.3 GPa for the soft orientation.

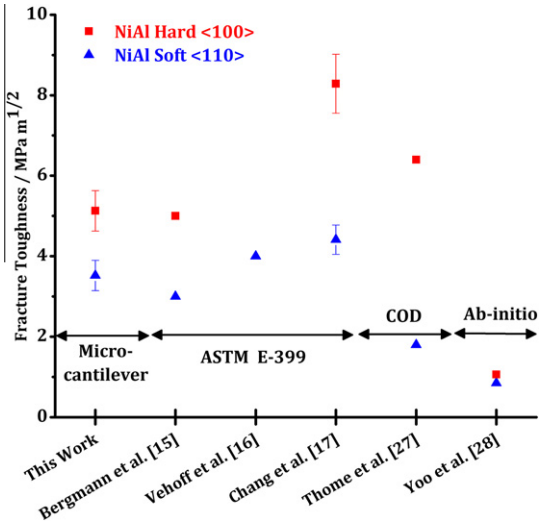

Fig. 6. Fracture toughness of NiAl crystals in "soft" and "hard" orientations from the micro-cantilver beam experiments and corresponding literature values from different testing methods. The ASTM E-399 tests refer to three- and four-point bend experiments and the Crack Tip Opening Displacement (COD) measurements were performed on macroscopic three-point bend specimens. The ab-initio values were taken from first-principles calculations.

4. Discussion

4.1. FIB milling and sample geometry

In the following, the validity of the microscopic fracture toughness test is discussed. The calculated geometry factor shows no dimensional dependency, hence slight changes of the aspect ratio (e.g. B/W ratio) during FIB milling will not falsify the fracture toughness results. Even though the notch tip radii varies and ranges from 70 nm to 120 nm, the scattering in fracture toughness is quite small and seemingly not influenced by the size of the notch tip radius. The fracture toughness values for the tested micro-cantilever specimens show surprisingly a good agreement with the literature values determined using ASTM 399 standard for plane-strain fracture toughness. However, the micron-sized specimens are far too small for plane-strain condition, when considering ASTM standard sample dimensions (Eq. (3)). Therefore we discuss the fracture behavior of the specimens and consider the size of the plastic zone with respect to the small sample thickness. In Fig. 8, SEM images of the cracked NiAl crystals in "soft" orientation and "hard" orientation are shown. In both cases, straight cracks along the direction of the notch are observed. This straight crack path is a good indication for the fulfillment of the plane-strain condition. For plane-stress or mixed-mode condition crack propagation at an angle of 45° is expected [29], which was not observed in this case. Before brittle crack propagation, some crack tip opening is visible (Fig. 5b), indicating limited crack tip plasticity for the "soft" orientation.

Since the cantilevers were prepared by FIB milling, some damage, like implantation of Ga^+-ions or storage of

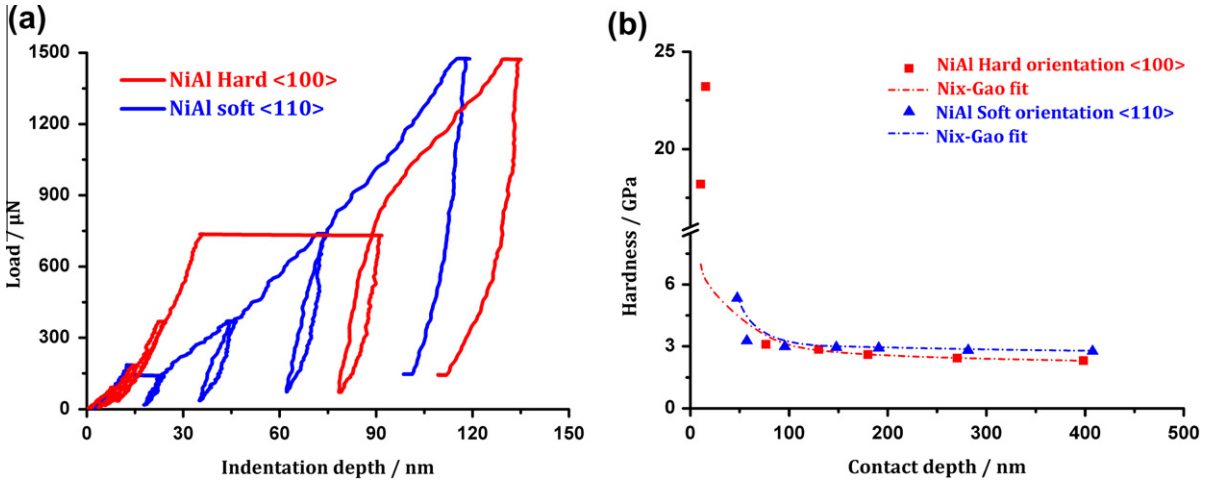

Fig. 7. Local mechanical properties of NiAl probed by nanoindentations: (a) load vs. indentation depth curves for "hard" ⟨100⟩ and "soft" ⟨110⟩ orientations; (b) hardness as a function of contact depth along "hard" ⟨100⟩ and "soft" ⟨110⟩ orientation of NiAl single crystals.

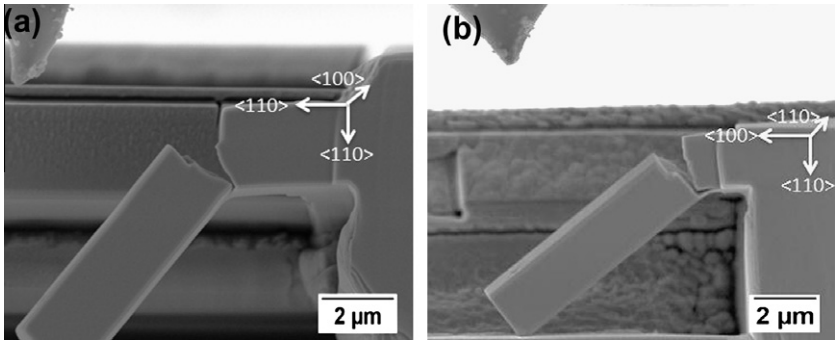

Fig. 8. SEM images of crack propagation along the notch direction for (a) soft orientation ⟨110⟩ and (b) hard orientation ⟨100⟩.

dislocations at the surface of the specimens, is expected. From previous work it has been shown that FIB damage is quite important concerning dislocation nucleation and size-dependent strength of micro-pillars [30]. A FIB-prepared molybdenum single crystalline micro-pillars showed a softening and the theoretical strength of the crystal was not reached. For the cantilevers, a softening of the samples would lead to an enhanced plasticity at the crack tip and could thus lead to a more ductile behavior, which was not found. Final milling of the notches was performed at 5 pA, therefore FIB damage seems not to be crucial.

4.2. Small sample dimensions

For discussing the fracture behavior of the small-scale NiAl specimens, different size effects, the orientation of the samples as well as the crack tip milling procedure need to be considered. Since the samples as well as the crack tip milling procedure are single crystalline and small with respect to the size of the plastic zone, the stored dislocation density is thought to be small as well. This is also causing the observed pop-in behavior in the load–displacement data for the "hard" orientation, followed by a small depth-dependent hardness. Dislocation nucleation required for initiating plastic deformation is inhibited and the material exhibits a high strength. The "soft" orientation on the other hand shows a distinct indentation size effect in a depth range <100 nm, with a much lower pop-in load. There the material strength is influenced by the indentation size effect.

For the "hard" orientation, no plastic influenced is observed at the crack tip; the material behaves thus elastically and fails in a brittle manner. The required stress for the nucleation of dislocations at the crack tip is thus larger than the local fracture stress. The "soft" orientation behaves quite differently; there, crack tip plasticity is found (see Fig. 4). Still the material fails in a brittle manner. To understand this behavior, the expansion of the plastic zone together with the work hardening at the crack tip needs to be discussed. Considering a macroscopic yield stress of 150 MPa for the "soft" and 1400 MPa for the "hard" orientation [21], a plastic zone size in the range of 58 µm for "soft" and 1 µm for the "hard" orientation is expected (Eq. (2)). The size of the plastic zone lies well above the specimen thickness for the "soft" orientation. In the case of the "hard" orientation the thickness of the specimens is close to the size of the plastic zone calculated for the plane-strain state.

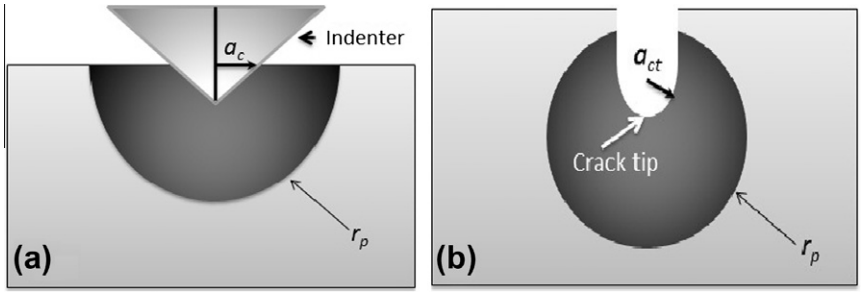

Fig. 9. Schematic illustration of the similarity between the plastic zone size and strain gradients for indentation and fracture: (a) indentation – contact radius a_c and size of the plastic zone r_p; (b) fracture – crack tip radius a_{ct} and size of the plastic zone r_p.

Table 1
Minimum critical thickness for the prediction of plane-stress, plane-strain state and the ratio of $K_{IC}^{plane-stress}$ to K_{IC} for hard and soft orientation calculated using macroscopic and local flow stress from Eq. (5).

	E (GPa)	$\sigma_Y = H/C$ from hardness (MPa)	Plastic zone size t_1 (μm) from hardness	ASTM criteria t_2 (μm) from hardness	σ_Y Macroscopic (MPa)	Plastic zone size t_1 (μm)	ASTM criteria t_2 (μm)	$\frac{K_{IC}^{plane-stress}}{K_{IC}}$
Soft	175	1800	0.4	9.6	150	58	1378	1.1
Hard	87	1800	0.9	20.2	1400	1	33	1.0

For the small notch radii, size effects due to strain gradients at the crack tip could also play a role. It is well known that close to the crack tip, strain gradients can lead to a substantial increase in the local flow stress of the material [24]. Hutchinson et al. showed that the local stress field close to the crack tip can reach values up to ten times the yield stress of the material, depending on the internal material length scale [24]. The local flow stress is thus quite important for the fracture behavior and it might deviate substantially from the macroscopic flow stress.

For estimating the expected local flow stress in the material due to strain gradient effects, the plastic zone at the crack tip is compared to the plastic zone found during indentation (see Fig. 9). The stress state at the crack tip is tensile in nature while compressive stresses dominate during nanoindentation. With indentations, however, the deformation resistance of the material at small length scales is easily assessed [31]. The magnitude of the strain gradients might also be different in both cases. However, here we propose using the local hardness for estimating the local flow stress of the material at the crack tip. Fig. 9 illustrates the geometric assumption that the contact radius of the indenter, a_c, is comparable to a crack tip radius, a_{ct}. In this case Eq. (6) can be rewritten to estimate the local yield stress σ_Y at the crack tip using Tabor's relationship:

$$\sigma_Y(a_{ct}) = \frac{H(a_c)}{C}, \quad \text{for } a_{ct} = a_c \tag{6}$$

where a_c is the radius of the indenter and a_{ct} is the radius of the crack tip.

The FIB made crack tips exhibit radii of $a_{ct} = 70$–120 nm, which is equal to a contact depth of 26–44 nm. These contact depths fall in a range where NiAl shows a hardness of 5.4 GPa for the "soft" orientation. The flow stress at this hardness value is thus estimated as 1.8 GPa It is important to note that this value doesn't represent the yield stress on the active slip system causing plastic deformation at the crack tip. In the case of the "hard" orientation a big pop-in displacement could not lead us to calculate the value of hardness at comparable notch radii. Therefore it is assumed that the material behaves purely elastic and no plasticity is expected. The hardness value of "soft" orientation was used for estimating the size of the plastic zone t_1 and the minimum specimen thickness t_2 for both orientations (Table 1). Values of $t_1 = 0.4$ μm for the "soft" and $t_1 = 0.9$ μm for the "hard" orientation are found, which are smaller than the specimen thicknesses but still not large enough to fulfill the ASTM (399) criteria of creating a plane-strain state, i.e. $t_1 < B/25$. The samples are thus tested in a mixed-mode condition and the reported fracture toughness values are lying inside the linear transition region according to the Anderson model [19]. The approximation provided by Broek and Vlieger [23] is used for assessing the ratio of $K_{IC}^{plane-stress}$ to K_{IC} (Eq. (4)) (Table 1). To calculate this approximation a fracture strain of $\varepsilon_f = 2\%$ [21,22] and, yield stress σ_Y values from nanoindentations and $E\langle 100\rangle = 87$ GPa for the "hard" and $E\langle 110\rangle = 175$ GPa [32] for the "soft" orientation are used. The estimated ratios for both orientations give roughly an $< 10\%$ difference for $K_{IC}^{plane-stress}$ to K_{IC}. Possible changes in the stress state have thus only a small effect on the fracture toughness.

Several reasons are thus responsible for the brittle fracture of the micron-sized NiAl cantilevers. First, the samples have a low initial dislocation density; the "hard" orientation requires a large stress for dislocation nucleation, favoring thus brittle fracture [28], as can also be seen from

the large pop-in loads in Fig. 7. The "soft" orientation on the other hand exhibits crack tip plasticity. Vehoff et al. observed remarkable dislocation activity at the crack tip in NiAl single crystals [16]. Dislocations are thus mobile and easily nucleated for the "soft" orientation, as can be seen in Fig. 5, as well as in the nanoindentation data. This is also confirmed by in situ TEM crack propagation experiments by Baither et al. on hard and soft oriented NiAl single crystals [33]. They found that the hard orientation exhibits only a limited amount of dislocation activity in the vicinity of the crack path, resulting in an instantaneous crack extension. For the soft orientation, a confined, but much larger plastic zone with high dislocation densities was observed at the crack tip prior to crack propagation. This is also in agreement with the findings here: Strain gradients acting at the crack tip can cause such high local dislocation densities causing brittle failure. The measured fracture toughness is thus comparable to the macroscopic fracture toughness values of NiAl reported in the literature [15–17].

Further investigations of the proposed strain gradient effects on the fracture behavior need to be tested on different materials in order to predict a solid correlation between micron-scale fractures to the bulk fracture experiments. For this reason a variety of metals and alloys ranging from ductile to brittle in nature and different specimen geometries are in the process of being tested. Furthermore the crack tip radius, the notch milling procedure as well as specimen size effects might influence the measured fracture toughness values.

5. Conclusion

A method for the investigation of the fracture toughness of micron-sized cantilevers prepared by FIB milling is described. A slightly varying B/W ratio during FIB milling doesn't change the calculated geometry factor $f(a/W)$ and thus the measured fracture toughness. (see Fig. 3b). The measured fracture toughness values are found to be 3.52 ± 0.29 MPa m$^{1/2}$ for the "soft" and 5.12 ± 0.50 MPa m$^{1/2}$ for the "hard" orientations, which is in good agreement with the macroscopic values [15–17,28]. When considering linear elastic fracture mechanics, it is shown that the tested specimen thicknesses are in the transition regime between plane-stress and plane-strain state. Consequently the estimation of $K_{IC}^{plane-stress}$ to K_{IC} ratio according to the Broek and Vlieger model [23] is calculated. The resulting difference of ~10% shows that NiAl "soft" and "hard" orientations have only a small thickness dependency of the plane-strain and plane-stress fracture toughness. For estimating the local flow stress at the crack tip it is proposed to use yield stress levels measured from nanoindentation experiments for the prediction of the size of the plastic zone t_1. The flow stress, σ_Y, at the crack tip faces strong strain gradients, which can be approximated with the help of nanoindentations. Hence the flow stress at the crack tip $\sigma_Y(a_{ct})$ is taken as one third of the hardness measured for the contact radius, which is equivalent to the notch radius (see Eq. (6)). The brittle fracture of the NiAl is based on two effects: first the high stresses required for dislocation nucleation, and secondly the large local stresses due to strain gradients at the crack tip.

Acknowledgements

Benoit Merle is thanked for helpful discussions on fracture mechanics. Verena Maier and Hamad ur Rehman are thanked for helping in nanoindentation measurements. Sarfraz Ahmed is highly acknowledged for assisting in finite element simulations.

References

[1] Nix WD, Gao H. J Mech Phys Solids 1998;46:411.
[2] Durst K, Göken M, Pharr GM. J Phys D Appl Phys 2008;41.
[3] Lilleodden ET, Nix WD. Acta Mater 2006;54:1583.
[4] Kiener D, Grosinger W, Dehm G, Pippan R. Acta Mater 2008;56:580.
[5] Tsuchiya T, Inoue A, Sakata J. Sens Actuat A Phys 2000;82:286.
[6] Halford TP, Takashima K, Higo Y, Bowen P. Fatigue Fract Eng Mater Struct 2005;28:695.
[7] Schweitzer EW, Göken M. J Mater Res 2007;22:2902.
[8] Merle B, Göken M. Acta Mater 2011;59:1772.
[9] Uchic MD, Dimiduk DM, Florando JN, Nix WD. Science 2004;305:986.
[10] Volkert CA, Lilleodden ET. Philos Mag 2006;86:5567.
[11] Haiford TP, Rudinal D, Takashima K, Higo Y. The effect of sample preparation upon the fracture toughness of microsized TiAl, vol. 297–300IV; 2005. p. 2416.
[12] Matoy K, Schönherr H, Detzel T, Schöberl T, Pippan R, Motz C, et al. Thin Solid Films 2009;518:247.
[13] Matoy K, Detzel T, Müller M, Motz C, Dehm G. Surf Coat Technol 2009;204:878.
[14] Di Maio D, Roberts SG. J Mater Res 2005;20:299.
[15] Bergmann G, Vehoff H. Mater Sci Eng A 1995;192–193:309.
[16] Vehoff H, Ochmann P, Göken M, Große Gehling M. Mater Sci Eng A 1997;239–240:378.
[17] Chang KM, Darolia R, Lipsitt HA. Acta Metall Mater 1992;40:2727.
[18] Standard test method for plane-strain fracture toughness of metallic materials. E 399-90. ASTM International; 1997.
[19] Anderson WE. Some designer-oriented views on brittle fracture; 1969.
[20] Irwin GR. Fracture. Berlin: Springer-Verlag; 1958.
[21] Noebe RD, Bowman RR, Nathal MV. Int Mater Rev 1993;38:193.
[22] Ebrahimi F, Shrivastava S. Acta Mater 1998;46:1493.
[23] Broek D, Vlieger H. The thickness effects in plane-stress fracture toughness. Amsterdam: National Aerospace Institute; 1974.
[24] Wei Y, Hutchinson JW. J Mech Phys Solids 1997;45:1253.
[25] Durst K, Franke O, Böhner A, Göken M. Acta Mater 2007;55:6825.
[26] Tabor D. The hardness of metals. Oxford: Oxford University Press; 1951.
[27] Thome F, Göken M, Vehoff H. Intermetallics 1999;7:491.
[28] Yoo MH, Fu CL. Mater Sci Eng A 1992;A153:470.
[29] Broek D. Elementary engineering fracture mechanics; 1986.
[30] Lowry MB, Kiener D, Leblanc MM, Chisholm C, Florando JN, Morris Jr JW, et al. Acta Mater 2010;58:5160.
[31] Backes B, Huang YY, Göken M, Durst K. J Mater Res 2009;24:1197.
[32] Rusovic N, Warlimont H. Phys Status Solidi (A) Appl Res 1977;44:609.
[33] Baither D, Ernst F, Wagner T, Rühle M, Bartsch M, Messerschmidt U. Intermetallics 1999;7:479.